Research in Astronomy and Astrophysics, 22:045001 (10pp), 2022 April https://doi.org/10.1088/1674-4527/ac4d21

The Study of Unusual Emission from PSR B1859+07 using FAST

Lin Wang[1,3], Ye-Zhao Yu[1,2], Feifei Kou[5], Kuo Liu[4], Xinxin Wang[6], and Bo Peng[1]
[1] CAS Key Laboratory of FAST, National Astronomical Observatories, Chinese Academy of Sciences, Beijing, 100101, China; pb@bao.ac.cn
[2] Qiannan Normal University for Nationalities, Duyun, 558000, China; yuyezhao@foxmail.com
[3] School of Astronomy and Space Science, University of Chinese Academy of Sciences, Beijing, 100049, China
[4] Max-Plank-Institut für Radioastronomie, Auf dem Hügel 69, Bonn, D-53121, Germany
[5] Xinjiang Astronomical Observatories, Chinese Academy of Sciences, Urumqi, 830011, China
[6] United World College of Changshu China, Changshu, 215500, China
Received 2022 January 5; revised 2022 January 14; accepted 2022 January 17; published 2022 March 17

Abstract

We present simultaneous broad-band radio observations on the abnormal emission mode from PSR B1859+07 using the Five-hundred-meter Aperture Spherical radio Telescope (FAST). This pulsar shows peculiar emission, which takes the form of occasional shifts of emission to an early rotational phase and mode change of emission at the normal phase. We confirm all these three emission modes with our data sets, including the B (burst) and Q (quiet) modes of the non-shifted pulses and the emission shift mode with a quasi-periodicity of 155 pulses. We also identify a new type of emission shift event, which has emission at the normal phase during the event. We studied polarization properties of these emission modes in detail, and found that they all have similar polarization angle curve, indicating the emissions of all these three modes are from the same emission height.

Key words: pulsars: general – pulsars: individual (B1859+07) – methods: observational

1. Introduction

The study of pulsar emission is one of the most important subjects in pulsar astronomy, for the main purpose of understanding the underlying physics of the emission process. This has been carried out extensively based on some peculiar emission phenomena such as sub-pulse drifting, nulling, mode changing and so forth. Some of these phenomena have been seen and studied for years and can now be partially explained by theories of pulsar emission. However, some phenomena are still poorly understood, which requires more observational facts to build a theoretical system that is consistent with the observation. A remarkable phenomenon of such is called "emission shift", "swoosh" or "flare" in the literature (e.g., Rankin et al. 2006; Han et al. 2016; Perera et al. 2016; Wahl et al. 2016), first identified by Rankin et al. (2006) in PSRs B0919+06 and B1859+07. This phenomenon is seen as emission from subsequent rotations gradually arriving in an earlier pulse phase, then lasting for tens of pulse periods and finally gradually returning back to the usual emission pulse phase. A quasi-periodicity of the emission shift behavior was discovered in PSR B1859+07 and very likely in PSR B0919+06 by Wahl et al. (2016). Since then, some hypotheses have been raised to explain this peculiar emission phenomenon in these two pulsars (Wahl et al. 2016; Yuen & Melrose 2017; Gong et al. 2018; Rajwade et al. 2021). Yu et al. (2019) studied the emission shift events of PSR B0919+06 using multi-frequency Five-hundred-meter Aperture Spherical radio Telescope (FAST) data sets in detail, and found that there might be correlations between this peculiar emission behavior and the pulsar profile changing to some extent. However, the underlying physics of this phenomenon has yet to be revealed.

PSR B1859+07 has a spin period of 0.64 s and a high dispersion measure (DM) of 252.8 cm^{-3} pc, and is known for its abnormal emission mode as mentioned above. In addition to the emission shift, it has two slightly different profile shapes in its normal emission state. Perera et al. (2016) reported that its profile modulation corresponds to a quasi-periodic variation of spin frequency derivative with a period of 350 days. It is similar to PSR B0919+06 in that two emission states in the normal phase correlate to a quasi-periodic spin frequency switching (Lyne et al. 2010). However, the emission shift states of both PSR B1859+07 and PSR B0919+06 are not correlated to their spin frequency derivatives. Further studies of the emission shift event are then necessary to investigate whether it is linked to any characteristics of the pulsar.

Taking advantage of the excellent performance of FAST on individual pulse study for radio pulsars (Wang et al. 2019), we examined emission states of PSR B1859+07. In Section 2, we introduce the details of our observation and the data analysis of this work. We present our results, including the emission shift state, profile modulation and polarization in Section 3. We further discuss the possible correlations between our results and the pulsar characteristics in Section 4 and summarize the conclusions of this work in Section 5.

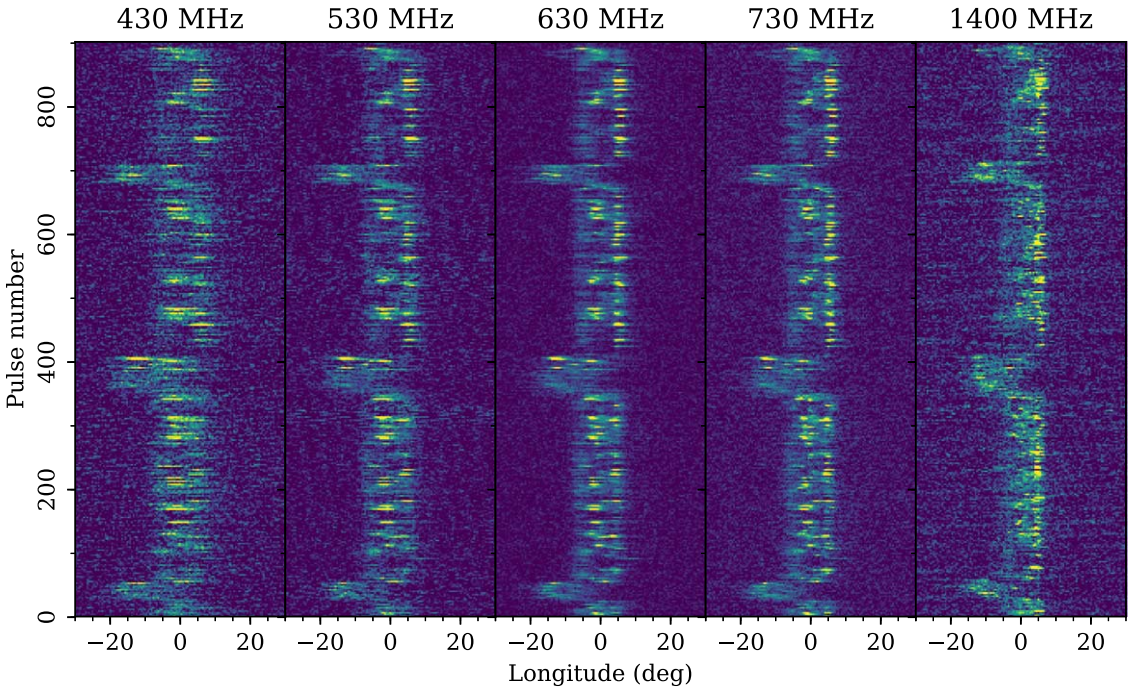

Figure 1. The pulse-stack of PSR B1859+07 simultaneously observed with FAST using the UWB receiver in February 2018. The panels from left to right are data at center frequencies of 430, 530, 630, 730 and 1400 MHz, respectively. The bandwidth of the first four panels is 100 MHz and that of the fifth panel is 300 MHz. Three emission shift events are displayed at each frequency.

Table 1
Observational Parameters

Date (year-month-day)	MJD day	Receiver	Pols	Length (pulses)	Events	Shift (pulses)	B mode (pulses)	Q mode (pulses)
2018 01 23	58141	UWB	2	2773	13	411	1594	768
2018 02 09	58159	UWB	2	2811	15	421	1635	755
2018 08 28	58358	19 beam	1	2795	12	466	1537	792
2019 12 03	58820	19 beam	4	5590	29	850	1543	3197
2020 11 22	59175	19 beam	4	8800	55	1541	1980	5279

Note. In the polarization column, the numbers refer to 1: one of the two linear polarization channels; 2: two linear polarization channels; 4: full polarizations. Events are the number of emission shifting events captured in the data set. UWB is the ultra-wide bandwidth receiver and 19 beam refers to the 19 beam receiver.

2. Observations and Data Reduction

We observed PSR B1859+07 with FAST at multiple frequencies starting from January 2018. Before May 2018, an Ultra-Wideband receiver (UWB) covering frequency range of 270–1620 MHz (Jiang et al. 2019) was used, and we observed PSR B1859+07 twice using the UWB. The signal from the UWB was originally filtered into two subbands, 270–1000 MHz (the low-band) and 1000–1620 MHz (the high-band), to minimize the influence of strong interference (Zhang et al. 2020). Both of the two subbands were then sent to a Reconfigurable Open Architecture Computing Hardware 2 (ROACH 2)[7] unit, and were sampled at Nyquist frequency, digitized into 8 bit real samples with dual polarization, packetized and stored on a hard-drive device in PSRFITS format. The sampling time and channel bandwidth of the UWB data are 100 μs and 0.25 MHz, respectively.

After May 2018, the UWB was replaced by a 19 beam receiver with frequency spanning 1050–1450 MHz (Jiang et al. 2020). We observed PSR B1859+07 employing the 19 beam receiver on 2018 August 28, 2019 December 3 and 2020 November 22. The 19 beam data were also sampled and

[7] https://casper.berkeley.edu/

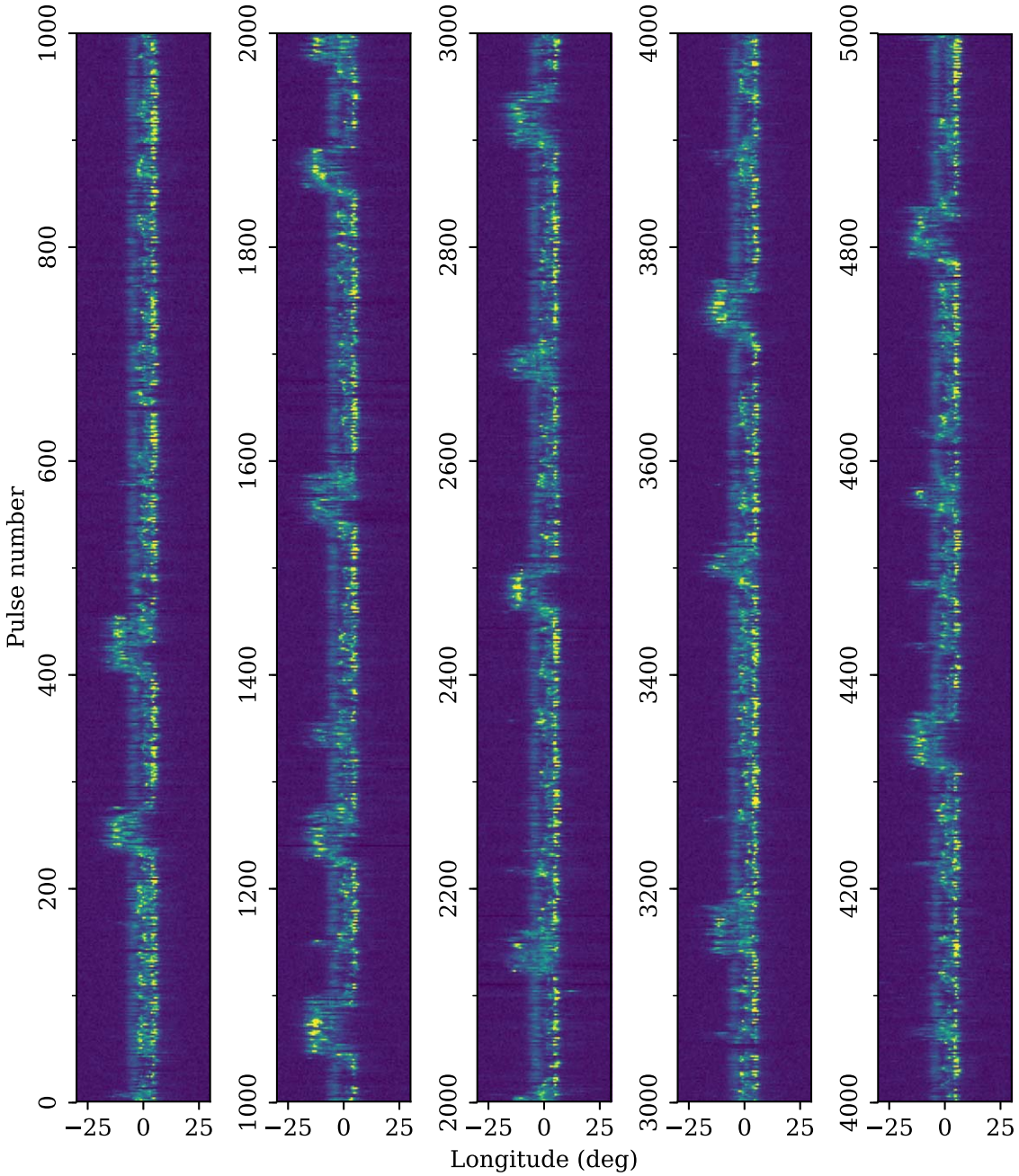

Figure 2. The pulse-stack of B1859+07 observed with FAST using the 19 beam receiver in November 2020. Both long and short duration emission shift events are displayed.

digitized utilizing the ROACH unit, then output to 8 bit PSRFITS files. The observation made in August 2018 was recorded with only one polarization due to a hardware issue, and the other two data sets were output with full polarization. The time resolution and channel bandwidth of the data sets observed in August 2018 and December 2019 were 49.152 μs and 122 kHz, respectively. The last 19 beam data were sampled with time resolution of 196.608 μs and channelized with channel bandwidth of 122 kHz. Before the observations made both in December 2019 and November 2020, the telescope pointed to an off-source region and tracked for 2 minutes. During the off-source observations, a noise diode with a period of 0.2 s and temperature of 10 Kelvin was injected. The off-source data were recorded with the same time and frequency

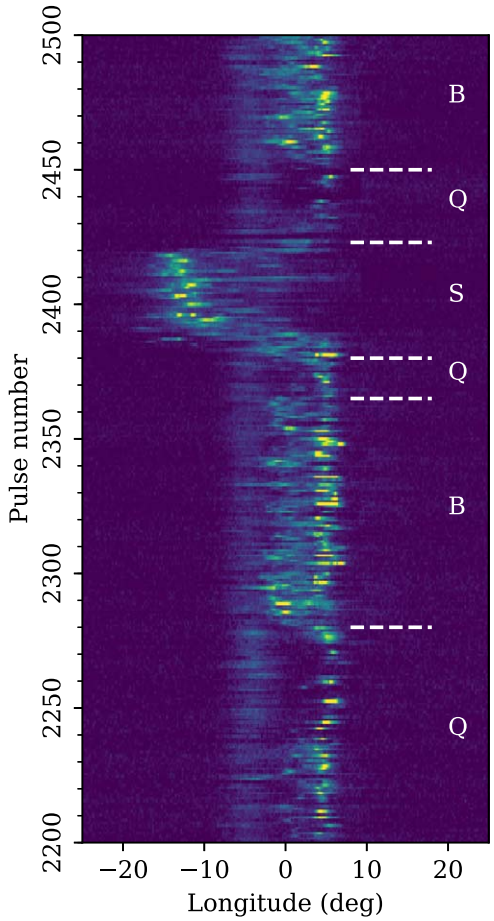

Figure 3. A zoom-in example for the emission shift event of B1859+07 observed with FAST using the UWB receiver in August 2018. The B and Q modes are marked with "B" and "Q", respectively. "S" refers to the emission shift event.

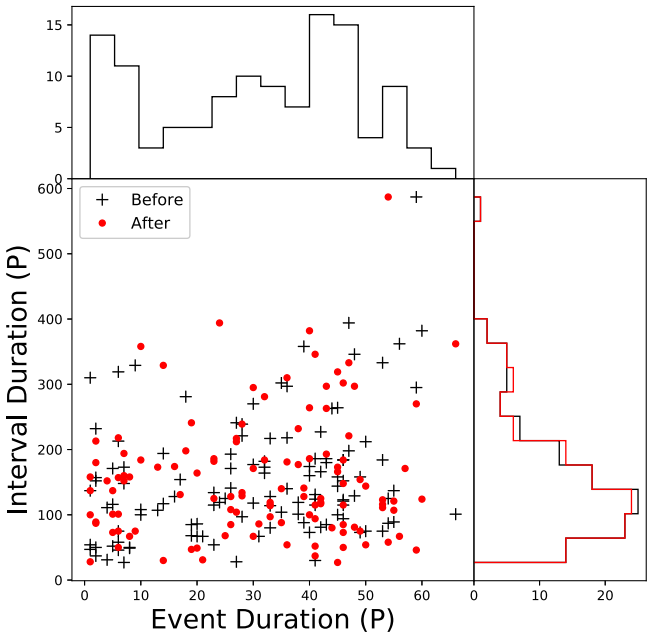

Figure 4. Distribution of the event duration and their interval duration for the 120 emission shift events. The interval duration refers to the time between two adjacent events. In the lower-left panel, the red points are the events with interval duration relative to their former events, and the black crosses are the events with interval duration relative to their later events. The top panel is the distribution of the event duration. The lower-right panel is the distribution of the event interval duration; 30 events have duration shorter than 15 periods, while 21 of them are captured in the data set observed on 2020 November 22.

resolution. A summary of all these observations is listed in Table 1.

All five data sets were dedispersed at the best DM of PSR B1859+07 and folded using the pulsar software package DSPSR (van Straten & Bailes 2011). Each rotation was sampled using 1024 phase bins. After dedispersing and folding, we divided the low-band UWB data into 10 subbands and each has bandwidth of 50 MHz between 280–780 MHz. The subbands between 280–380 MHz were removed from this work due to strong radio interference. The high-band UWB data were analyzed as a whole between 1250–1550 MHz, as most of the data were contaminated by radio interference. The 19 beam observations made in December 2019 and November 2020 were polarization calibrated utilizing the pulsar software package PSRCHIVE (Hotan et al. 2004) after dedispersing and folding. In order to reduce the computing time, we summed every eight frequency channels, resulting in a final channel bandwidth for these two data sets of 976 MHz. No polarization calibration was operated on the data set from August 2018 due to a hardware issue. We then searched for the emission shift events by examining the energy in the pulse region of $-20^\circ \sim -10^\circ$ (Figure 1) among all these individual pulses. We identified the emission shift event as the significance of the energy in the region of $-20^\circ \sim -10^\circ$ when being greater than 7σ.

3. Results

3.1. Emission Shift Events

We generated 22,769 individual pulses in total, and captured 124 emission shift events. Figures 1 and 2 demonstrate examples of the emission shift events captured in the data sets observed in February 2018 and November 2020 at different frequencies, respectively. The former data set is from the UWB receiver and the later is from the 19 beam receiver. Figure 3 shows the details of one of the emission shift events. The emission from subsequent rotations gradually arrives in earlier pulse phase, then lasts for tens of pulse periods and finally gradually returns back to the normal emission pulse phase. We analyzed durations of the events and the time interval between two adjacent events in Figure 4. The durations of most of the emission shift events are longer than 15 pulse periods with an approximate median value of 50 pulse periods. Only 30 shift

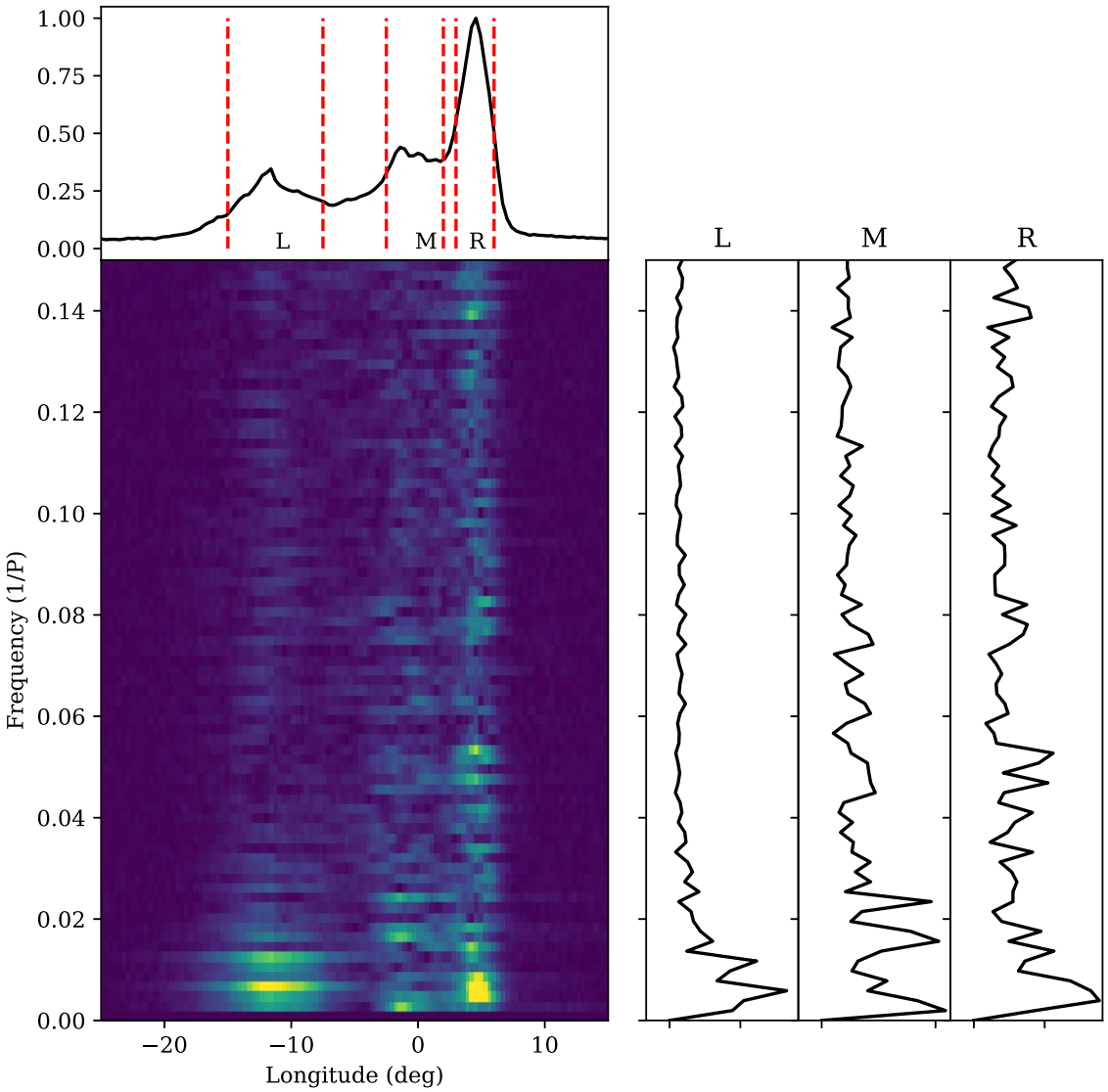

Figure 5. The 2D fluctuation spectrum of B1859+07 observed using FAST on 2020 November 22. The summed spectra of L, M and R are shown in the right panels from left to right, respectively. These summed spectra indicate the L, M and R regions have low frequency peaks of ∼0.006, ∼0.016 and ∼0.006 cycles per period, which indicate quasi-periods of ∼160, ∼60 and ∼160 pulsar periods, respectively.

events are shorter than 15 pulse periods, and 21 out of 30 are from the data set observed in November 2020. We also noticed a median value of the time interval of 155 pulse periods. Using longitude-resolved fluctuation spectrum analysis, we found a quasi-periodicity of 160 pulse periods in the occurrence of these events as displayed in Figure 5. This agrees with the median of the time interval of the events, and is consistent with the 150 period periodicity reported in Wahl et al. (2016). Zooming into each emission shift event, we noticed a distinct type of these events. An example of such is displayed in Figure 6, where emission is present in both shifted and non-shifted pulse regions, and almost one third of the shifted events show behavior like this. The emission shift events appear simultaneously in all frequency bands of our data sets (see Figure 1). They are frequency-dependent (Figures 7 and 8), though this phenomenon is not significant in the individual pulses (Figures 1 and 2). We present the average profile of the shifted pulses in Figure 7, which shows complex components. The leading component is brighter at high frequency bands, and the intensity difference between components becomes less significant as observing frequency decreases. The offsets of the shifted pulse profiles with respect to the non-shifted ones display frequency-dependence. This frequency-dependence is contrary to that of PSR B0919+06, where the maximum offset of shifted pulses increases with deceasing frequency (Rajwade et al. 2021). In order to model this frequency-dependence, we

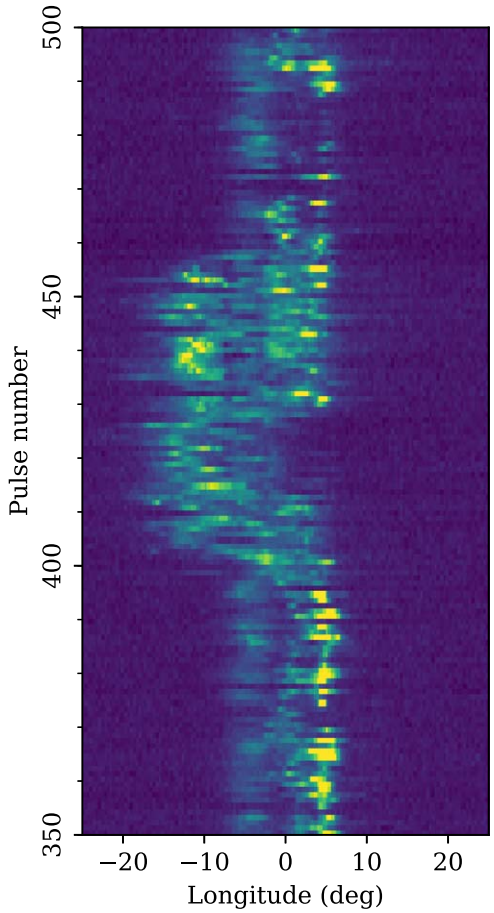

Figure 6. A zoom-in example for the emission shift event of B1859+07 observed with FAST using the 19 beam receiver in November 2020.

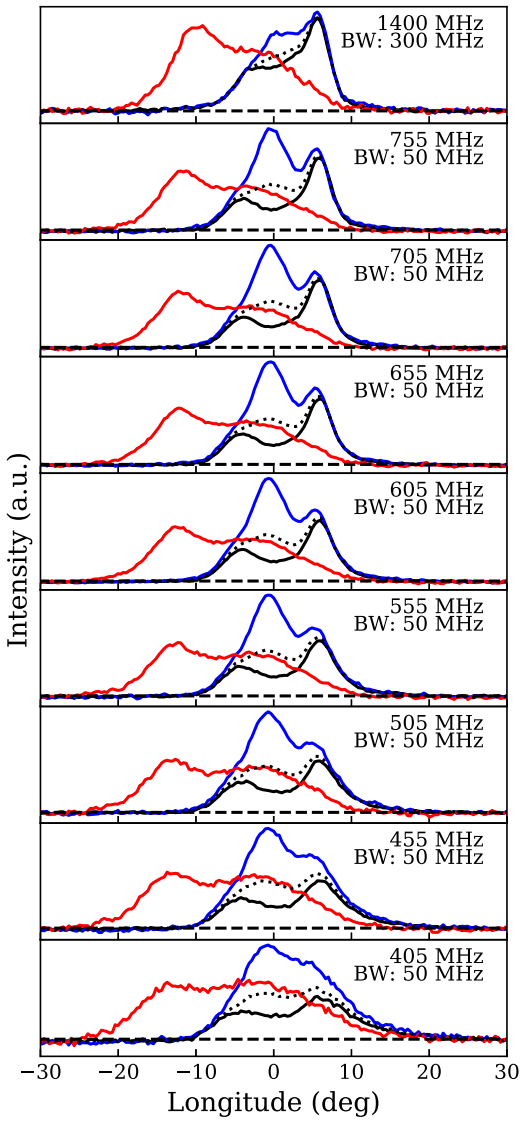

Figure 7. Normalized average profile at different frequencies of each emission state, including emission shift, B mode and Q mode. The data were observed on 2018 February 9 using the UWB receiver. The red solid and black dotted curves represent the average profiles of the emission shifted and non-shifted pulses, respectively. Black solid and blue curves are the profiles of Q and B modes, respectively, among the non-shifted pulses.

performed three-component fitting on these profiles, and measured the maximum offset between the peak of the shifted pulse profile and the non-shifted one in each frequency band. Then a power-law is applied to model the frequency-dependence of the offset (Ruderman & Sutherland 1975)

$$\Delta\theta = A\nu^{-\alpha} \quad (1)$$

where α is the separation index. We derived the power-law index $\alpha \sim 0.169(8)$ (see Figure 8).

3.2. Non-shifted Pulse Behavior

As depicted in Figure 3, the intensity around the longitude of "0°" fluctuates between a strong and weak state. These are two emission states within the group of non-shifted pulses. In order to distinguish these two states, we first generated a profile by averaging all the non-shifted pulses. A noise-free template was created by fitting von Mises functions to the integrated average profile. Then we selected the region between longitude $-2.^{\circ}5$ and $+2.^{\circ}5$, and compared the energy of all non-shifted pulses with the template in this region. The pulses that were brighter than the template in this region were defined as B (Burst) mode, otherwise the pulse would be classified as Q (Quiet) mode. Examples of these two modes are marked in Figure 3. An intriguing phenomenon is that almost all of the shift events are followed by a series of Q mode pulses in the data sets before 2020, while only half of shift events are seen to be followed by Q mode subsequent pulses in the data set observed in November 2020. We integrated the pulses of the B and Q modes in each frequency band and generated average profiles

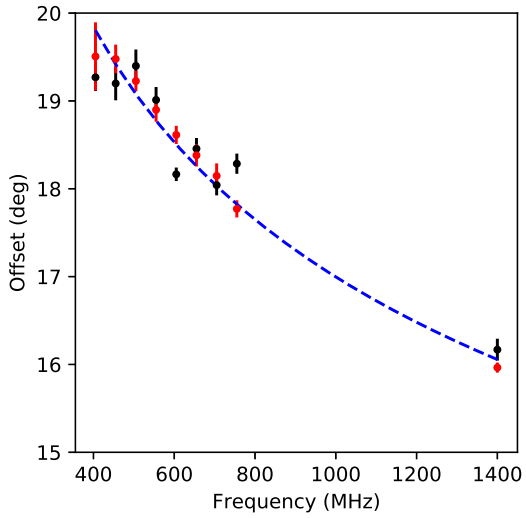

Figure 8. The offset between the non-shifted pulse profiles and the shifted pulse profiles as a function of observing frequency for PSR B1859+07. Each component is modeled by a Gaussian function and the offset is measured from the peak of shifted pulse profile to the non-shifted pulse profile. Black and red correspond to the data set observed on 2018 January 23 and 2018 February 9, respectively. All data points feature 1σ error bars. The blue dashed curve is the power-law fitting result.

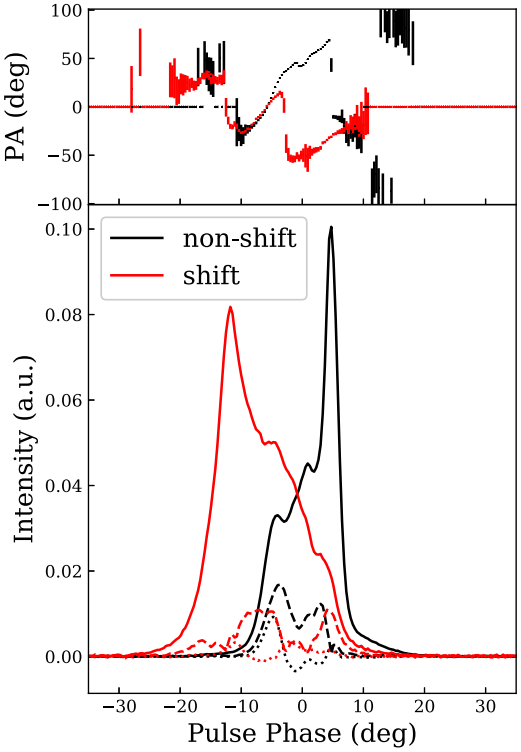

Figure 9. Polarization averaged profiles of B1859+07. The data considered here are from the observation using the 19 beam receiver on 2019 December 3. The upper panel shows the curve of the linear PA, Φ. The PA of emission shifted and non-shifted pulses are marked in red and black, respectively. In the bottom panel, red curves are averaged profiles for the emission shifted pulses and black curves are for the non-shifted pulses. The solid, dashed and dotted curves correspond to total I, linear polarization L and circular polarization V intensity, respectively. The intensity is in arbitrary unit (a.u.).

of these two modes in Figure 7, respectively. Both profiles of the two modes exhibit complex components, and each component shows evolution with frequencies. In the data sets with center frequency between $405 \sim 755$ MHz, the leading component of B mode is brighter than its trailing component, and the difference in intensity between the two components decreases as observing frequency decreases. The B mode displays a brighter trailing component at 1.4 GHz. The Q mode exhibits a brighter trailing component in all frequency bands, and the intensity difference between components decreases with decreasing frequency.

3.3. Polarization

Similar to the majority of pulsars, the polarimetry of an average profile in PSR B1859+07 is highly linearly polarized as demonstrated in Figure 9. Similar percentages of linear and circular polarizations are manifested in profiles of both shifted and non-shifted pulses. "Jumps" appear in the Polarization Angle (PA) curves of both shifted and non-shifted pulse profiles at slightly different longitudes, as demonstrated in Figure 9. Since the non-shifted pulses dominate between longitude of $-7^\circ \sim 7^\circ$, we plot the PA distributions of both shifted and non-shifted individual pulses in Figure 10. Two orthogonal polarization modes appear simultaneously in the non-shifted individual pulses at both sides of longitude 0°. For the non-shifted individual pulses, their orthogonal polarization modes are present simultaneously at both sides of longitude 0°. The dominate polarization mode switches between one and the other at the longitude around 8°, which results in the PA shift for the mean pulse profile (Figure 9). The polarized profiles of B and Q modes are displayed in Figures 11 and 12. The two emission modes have similar polarization properties, although the PA curve of B mode shows fluctuations around longitude of 0°. As done for shifted and non-shifted pulses, we analyzed the PA distribution of the B and Q modes. As displayed in Figure 10, the two modes have very similar PA curves, except that there are few Q mode pulses with PA around -40°.

4. Discussion

Tracing the emission and propagation of the pulsar signal, the emission shift events in principle could be resulting from asymmetry in the pulsar emission beam, the change of pulsar magnetosphere or dynamic effects around the pulsar (e.g., tidal effects from an ultra-compact binary). Wahl et al. (2016) and Gong et al. (2018) suggested that the emission shift events may reflect existence of an orbiting body. However, we suspect that this is unlikely to be the reason based on the work done on this

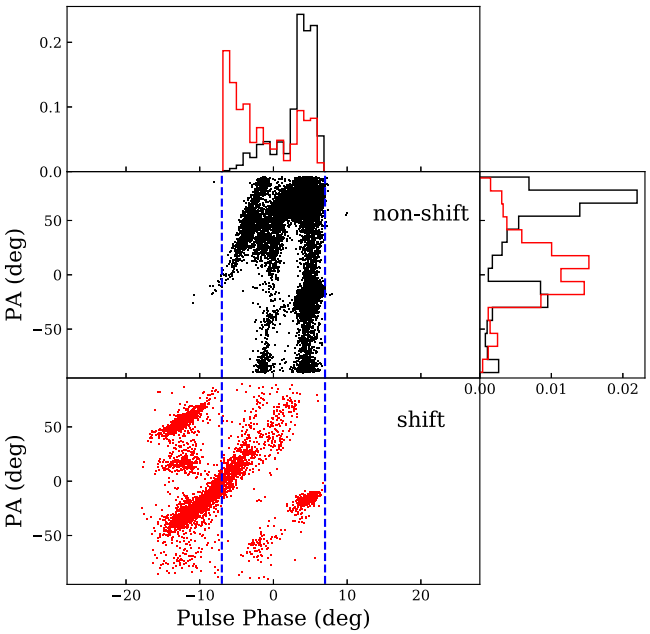

Figure 10. Polarization statistics of the shifted and non-shifted pulses of B1859 +07. The data set comes from the observation using the 19 beam receiver on 2019 December 3. Red and black represent the PA of shifted and non-shifted pulses, respectively. The top-left and right panels are the histograms of the normalized probability density distribution.

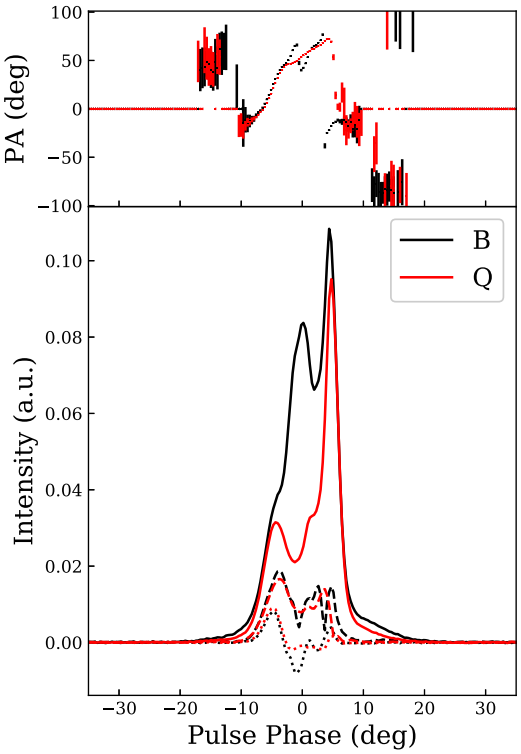

Figure 11. Polarization averaged profiles of PSR B1859+07. This data set comes from the observation on 2019 December 3. Black and red correspond to B and Q modes, respectively. In the lower panel, the solid, dashed and dotted curves are total I, linear polarization L and circular polarization V intensity, respectively. The upper panel shows the linear PA curves.

pulsar in the literature. If we assume this pulsar is a member of an ultra-compact system and the emission shift events are due to the tidal effect of the companion, the observed spin period derivative would be affected by the orbital motion and thus correlated with the events. However, Perera et al. (2016) investigated the link between the spin period derivative and the emission shift events, but no correlation was found therein. Thus the emission shift events in PSR B1859+07 are not likely linked to the orbital motion.

Based on radius-to-frequency mapping (RFM; Cordes 1978) in pulsars, the pulse profile is narrower at high frequency than that at low frequency. Earlier observations confirmed that the separation between components of a pulsar profile decreases with increasing frequency. The frequency dependence of the component separation can be described by Equation (1). Manchester & Taylor (1977) modeled this relationship for several pulsars, and found $0.08 \leqslant \alpha \leqslant 0.5$ when frequency is below 1.4 GHz. Our results reveal that the offset of the shifted pulse decreases with increasing frequency following the relationship of Equation (1), and we derived the power-law index $\alpha \sim 0.169(8)$ (see Figure 8). Intriguingly, PSR B0919 +06 is another pulsar known for its emission shift events, but shifted offset increases with increasing frequency (Rajwade et al. 2021). Obviously, the events from the two pulsars cannot be described simply using RFM. If we attribute the emission shift events of both PSRs B0919+06 and B1859+07 to different origins, the emission of PSR B1859+07 tends to be under the frame of RFM since the power-law index in Equation (1) from our result is in agreement with Manchester & Taylor (1977). If the emission shift events of the two pulsars have the same origin, it is likely that the shifted and non-shifted components have different radiation centers, thus Equation (1) is not applicable to describe the relationship between component offsets and frequencies. Rankin et al. (2006) explained the behavior of these two pulsars based on the core-cone model, claiming that the usual emission of these pulsars was due to a partially active cone. The leading part of the cone was inactive and active during the non-shifted and shifted emission modes respectively while the trailing part was the inverse. This scenario is not able to explain all the behaviors of these pulsars, such as the duration of the emission shift events. An alternative model was put forward to explain the emission features of these pulsars by Rajwade et al. (2021), based on the shrinking and expanding magnetosphere of the neutron star proposed in Timokhin (2010). Rajwade et al. (2021) explain the emission beam to be a patchy fan beam, and the polar cap region expands as the magnetosphere is shrinking thus changing the angle between the emission beaming direction and our line of

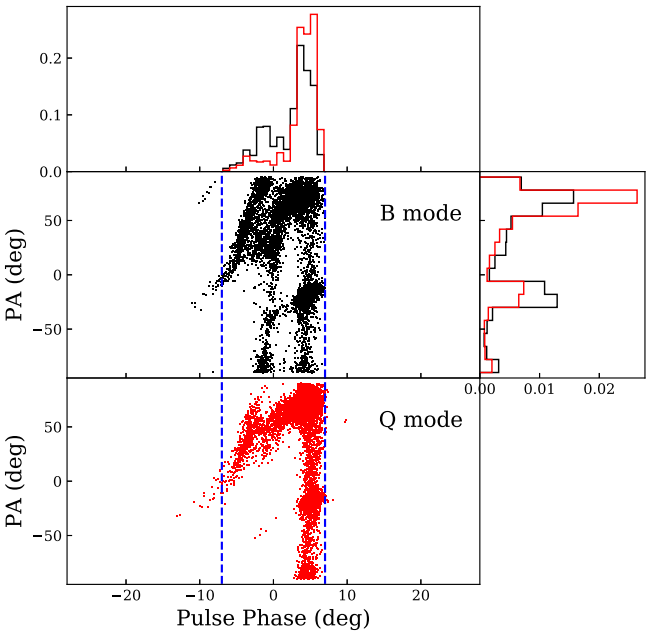

Figure 12. Polarization statistics of the B and Q modes of B1859+07. The data set comes from the observation using the 19 beam receiver on 2019 December 3. Red and black represent the PA of Q and B modes, respectively. The top-left and right panels are the histograms of the normalized probability density distributions.

sight (LOS). Emissions from different heights may stay in or out of the LOS depending on the scale of shrinking (see Figure 10 in Rajwade et al. 2021). A simple way to test whether this scenario is applicable is to measure the emission heights of the three emission states. While it is not easy to measure the emission heights, we can still parse this problem in a qualitative way. The PA reflects the direction of the magnetic field at the point of emission and PAs at the same pulse phase are in principle different due to aberration, retardation and field line distortion of a pulsar. Our results affirm that all the three emission modes have similar PA distributions, thus we suspect the emission at the same phase corresponds to similar emission height. The three modes are unlikely to result from the propagation effect which is a gradual process in the usual sense. The emission shift events with emission at both the shifted and non-shifted pulse regions are also difficult to explain by the model in Rajwade et al. (2021).

We noticed that components L and R have the same modulation periods of ∼160 pulse periods, while component M has the modulation period of 60 spin periods in Figure 5, and component L refers to the emission shift events. When the shift events occur, the source is usually bright in component L but faint in component R, which results in the same cadence of flux variation and thus leads to the same modulation period of L and R. Component M corresponds to the mode changing (B and Q modes) state, and no evidence indicates that the mode changing correlates to the emission shift events. Considering the different modulation periods between components M and the other components (L and R), it is likely that component M originated from different regions compared to components L and R. However, whether these emission modes are due to intrinsic change of radiative particles from the pulsar would be an interesting but challenging question. Further observations using high sensitivity telescopes, especially FAST, on a larger sample of this kind of pulsar would facilitate the solution to this question.

5. Summary

We present FAST observations of PSR B1859+07 at 400 ∼ 1400 MHz using the UWB receiver and 1.4 GHz using the 19 beam receiver. We study the emission shift events of PSR B1859+07 utilizing the simultaneously observed multi-frequency data, and ascertain that the shift events are frequency-independent. A quasi-periodicity of about 150 pulses was found by analyzing the event interval duration distribution. We discovered a new type of emission shift event with emission at both the shifted and non-shifted phases. We also identified the two emission states, the B and Q modes, in the non-shifted pulses. We analyzed the polarization properties of the three emission states, and found that the three modes have almost the same PA distribution. We argue that none of the models in the literature explains the phenomena of this pulsar well.

Acknowledgments

This work is supported by the National Key R&D Program of China under grant number 2018YFA0404703, the Open Project Program of the CAS Key Laboratory of FAST, NAOC, Chinese Academy of Sciences, and the Guizhou Education Department under Grant No. Qian Education Contract KY [2019]214. This work is supported by the West Light Foundation of the Chinese Academy of Sciences (No. 2018-XBQNXZ-B-023), the “Tianchi Doctoral Program 2021”. This work made use of the data from FAST (Five-hundred-meter Aperture Spherical radio Telescope). FAST is a Chinese national mega-science facility, operated by the National Astronomical Observatories, Chinese Academy of Sciences.

References

Cordes, J. M. 1978, ApJ, 222, 1006
Gong, B. P., Li, Y. P., Yuan, J. P., et al. 2018, ApJ, 855, 35
Han, J., Han, J. L., Peng, L.-X., et al. 2016, MNRAS, 456, 3413
Hotan, A. W., van Straten, W., & Manchester, R. N. 2004, PASA, 21, 302
Jiang, P., Tang, N.-Y., Hou, L.-G., et al. 2020, RAA, 20, 064
Jiang, P., Yue, Y., Gan, H., et al. 2019, SCPMA, 62, 959502
Lyne, A., Hobbs, G., Kramer, M., Stairs, I., & Stappers, B. 2010, Sci, 329, 408
Manchester, R. N., & Taylor, J. H. 1977, Pulsars (New York: W. H. Freeman)
Perera, B. B. P., Stappers, B. W., Weltevrede, P., Lyne, A. G., & Rankin, J. M. 2016, MNRAS, 455, 1071

Rajwade, K. M., Perera, B. B. P., Stappers, B. W., et al. 2021, MNRAS, 506, 5836
Rankin, J. M., Rodriguez, C., & Wright, G. A. E. 2006, MNRAS, 370, 673
Ruderman, M. A., & Sutherland, P. G. 1975, ApJ, 196, 51
Timokhin, A. N. 2010, MNRAS, 408, 2092
van Straten, W., & Bailes, M. 2011, PASA, 28, 1
Wahl, H. M., Orfeo, D. J., Rankin, J. M., & Weisberg, J. M. 2016, MNRAS, 461, 3740
Wang, H.-G., Qiao, G.-J., Du, Y.-J., et al. 2019, RAA, 19, 021
Yu, Y.-Z., Peng, B., Liu, K., et al. 2019, SCPMA, 62, 959504
Yuen, R., & Melrose, D. B. 2017, MNRAS, 469, 2049
Zhang, H.-Y., Wu, M.-C., Yue, Y.-L., et al. 2020, RAA, 20, 075